

Heterogeneous Multi-Rate mass transfer models in OpenFOAM[®]

Federico Municchi¹, Nicodemo di Pasquale¹, Marco Dentz², and Matteo Icardi^{1,*}

¹School of Mathematical Sciences, University of Nottingham, NG7 2RD, UK

²Institute of Environmental Assessment and Water Research (IDA-CSIC),
Barcelona, Spain

*Corresponding author: Matteo.Icardi@nottingham.ac.uk

Abstract

In this work, we present a numerical implementation of the Multi-Rate mass transfer (MRMT) model in the opensource finite volume library OpenFOAM[®]. Unlike other codes available in literature, the one we propose can be applied to general geometries and highly heterogeneous fields, where the parameters of the MRMT can arbitrarily vary in space. Furthermore, being built over the widely diffused OpenFOAM[®] library, it can be easily installed and modified, as well as run in parallel architectures. First, we briefly describe the structure of the *multiContinuumModels* library that includes the formulation of the MRMT based on the works of Haggerty and Gorelick [20] and Municchi and Icardi [30], and we verify our method against manufactured solutions. Furthermore, we show how heterogeneity plays a significant role in the mass transfer when permeability and porosity are represented using Gaussian random fields.

1 Introduction

Interests in porous media dates back to the middle of nineteenth century with the study of Darcy describing the law that brings his name [41]. The reasons for such a long and wide interest resides in the fact that porous media are present in a wide range of systems and applications, both as natural [43] or industrial synthetic media. Also environmental applications as risk and safety assessment of groundwater contamination [38, 37], reservoir storage, geothermal extraction, geological disposal of radioactive waste [31] and carbon dioxide require the study of fluid flow and solute transport in fractured crystalline rocks, reducing to modelling of porous media materials.

One of the peculiar characteristic of these systems is their heterogeneity, which results in non-equilibrium and memory effects. A porous medium can be described as a matrix of solid material in which a fluid phase moves. Usually, the fluid phase (mono or multi-component) is called the *mobile* region whereas the remaining part is the *immobile* region. It is often assumed that the dominant transport process in the immobile regions is the diffusion [29], while the mobile region can exchange mass and energy with the immobile one.

This heterogeneity, and the different transport processes between different regions, complicates the description of transport processes within porous media, and several methods were devised to mathematically describe these effects. Among the spectrum of methodologies, we want to recall:

Nomenclature

β_i	Capacity in the immobile region i	Ω_m	Mobile region
β_m	Capacity in the mobile region	$\widetilde{(*)}$	Favre averaging operator
\mathbf{u}	Velocity field	c_i	Concentration in the immobile region i
λ_{ik}	Eigenvalue for the immobile region i mode k	c_m	Concentration in the mobile region
\mathcal{D}_i	Effective diffusion coefficient for immobile region i	N_i	Number of immobile regions
\mathcal{D}_m	Effective diffusion coefficient for the mobile region	V	Reference volume
Ω_i	Immobile region i	V_i	Volume of immobile region i
		MRMT	Multi-Rate mass transfer

- The Dual-Porosity formulation, where the medium is modelled as two overlapping continua (mobile and immobile);
- The Integro-Differential formulation [22, 23, 10], which uses a mix of convolutions of state variables and memory functions to model the transport process to the immobile region/
- The Continuous Time Random Walk [3, 13, 5], which assumes a random walk in time and space for the movement of solute particles in a heterogeneous medium.

One of the formulation which received lots of attention in the past decades is the Multi-Rate Mass Transfer (MRMT) Model [34, 20, 21, 40, 18, 2] which can be seen as a generalisation of the dual-porosity model. In the MRMT one assumes the medium is composed by one mobile region and several immobile regions, which model the heterogeneity of the medium and the mass transfer between mobile and immobile regions is represented by a first-order mass transfer equation. The interest in the MRMT model stems also from the fact that all the formulations for the description of transport properties in porous media and heterogeneous system cited earlier are somewhat all equivalent [35]. The MRMT model is, in comparison with the others, the one with the most straightforward mathematical framework, and has the important property that allows localisation. The latter means that the properties of the heterogeneous systems can be described locally, by defining different immobile regions, without the need to define global quantities, which usually allow less flexibility in the description of these complex systems.

Several problems can be addressed withing the MRMT methodology, a fact that makes this framework extremely flexible and useful. The complexity of flow fields into highly heterogeneous medium (such as the porous media we are considering) modify the transport behaviour of solutes within the fluid. In these kinds of systems a non-Fickian diffusive behaviour one is observed [32]. The nature of the non-Fickian transport was extensively studied in literature [6, 4, 32], and its origin was found on the broad spectrum of transition times intrinsic to heterogeneous media[4].

An important environmental problem we are currently facing, is the high concentration of CO₂ in the atmosphere, due to entropic contribution (mainly energy production). One of the most promising strategies devised to reduce carbon emissions is the Carbon Capture and Storage (CCS) through gas hydrate and crystallization [36]. This process separates the CO₂ from fuel gas, by sequestration

in gas hydrate crystals (mainly water). It was observed that using porous media this process can be improved thanks to the much higher gas/water contact [1], and therefore a reliable model for transport properties in such systems becomes essential.

In dispersion of contaminants in aquifer and groundwater remediation, the dynamic of diffusion of chemical compounds (either contaminants or formulations created to reduce contamination) into the ground is studied. One of the way to perform *in situ* remediation which has recently gained lots of attentions, involves the injection of a reactive suspension of engineered nanoparticles to degrade transform, or immobilise the pollutants[17, 42]. Both the dynamic of the dispersion of the pollutant, and the transport of these nanoparticles [26] are dominated by the exchanging of mass or energy with a set of impermeable inclusions, which could be modeled through MRMT.

A first formulation of the numerical implementation of the MRMT model was presented in Silva et al. [35]. This approach can describe a wide range of non-equilibrium phenomena by using a model which is local in time. The variable referring to immobile zones are solved as explicit functions, avoiding the need of a discretisation of these regions. By assuming a functional form for the the concentration in the mobile region during each time increment (in the [35] it was assumed a linear behaviour), it is possible to explicitly integrate the first-order linear differential equations referring to the immobile regions. Therefore, in this formulation we need a spatial discretisation of the mobile regions, and the contribution of each immobile region can be included in the discretized (in time and and space) equations describing the evolution of the concentration in the mobile region.

In this work we propose a new numerical implementation of the MRMT model, based on the generalisation proposed in an earlier work of some of the authors [29]. This numerical implementation is written as a new library within the C++ opensource finite volume library OpenFOAM[®][33]. Our choice of OpenFOAM[®] was based on the fact that this code has a wide diffusion across industry and academia alike.

This paper is structured as follows: we first present the relevant equations and hypothesis for the generalized MRMT model by following the derivation reported in [29]. We then proceed to show how these equations can be implemented in OpenFOAM[®] by describing the structure of the new library we are presenting and we report some examples of application of our library in a number of test cases. We then proceed to draw some conclusions.

2 Mathematical formulation of the MRMT model

We present the essential features of the MRTM model and we refer to [29] for a complete derivation of the relevant equations. We consider an heterogeneous system of volume Ω composed by a *mobile* region, Ω_m , and a number N of *immobile* regions, Ω_i , with $i = 1, \dots, N$ such that $\Omega = \Omega_m \cup_{i=1}^N \Omega_i$ (see Figure 1).

We consider the advection-diffusion equation for a scalar field (which will be referred to as "concentration" for simplicity, even if it could be a temperature as well) in the mobile region, $c_m(\mathbf{x}, t)$, which reads as:

$$\frac{\partial c_m}{\partial t} + \nabla \cdot (\mathbf{u}c_m - \mathcal{D}_m \nabla c_m) = 0, \quad \mathbf{x} \in \Omega_m. \quad (1)$$

where \mathcal{D}_m is the diffusion coefficient in the mobile region. Furthermore, we consider N_i diffusion equations, one for each immobile region describing the concentrations $c_i(\mathbf{x}, t)$ in the i -th immobile region:

$$\frac{\partial c_i}{\partial t} = \mathcal{D}_i \nabla^2 c_i, \quad \mathbf{x} \in \Omega_i, \quad i = 1, \dots, N_i. \quad (2)$$

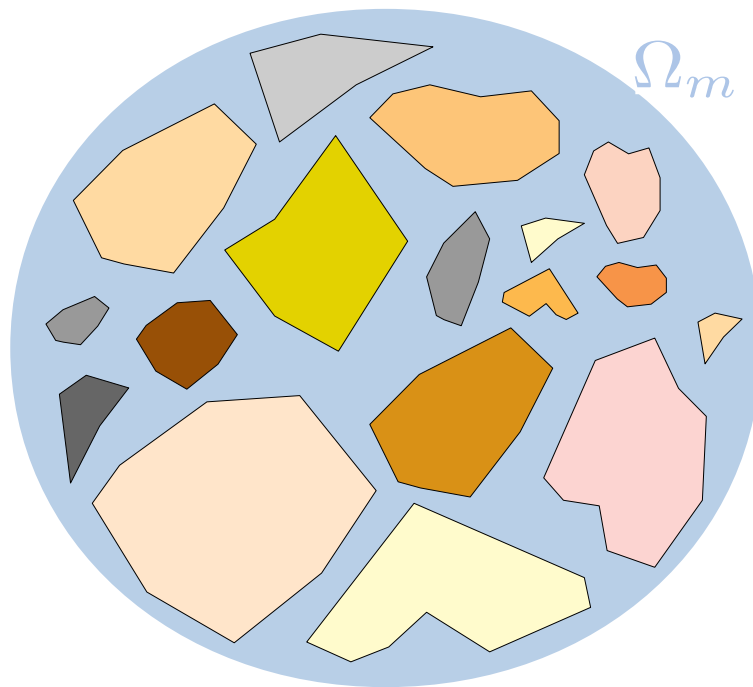


Figure 1: Representation of a typical fractured medium with a mobile region (light blue) and several immobile regions (colours) with different shape and composition. Fluid is flowing in the mobile region only, while contaminants (or heat) can diffuse within the immobile regions.

where \mathcal{D}_i is the diffusion coefficient in the i -th immobile region. Note that in previous equations we dropped the spatial and temporal dependence from c_m and c_i to simplify the notation. The equations describing the evolution of the concentration field in the mobile and the immobile regions must be coupled with the proper boundary conditions between the two kind of regions. Specifically, we impose continuity of fields and fluxes through the interfaces:

$$c_i = c_m, \quad \mathcal{D}_i \frac{\partial c_i}{\partial n} = \mathcal{D}_m \frac{\partial c_m}{\partial n}, \quad \mathbf{x} \in \partial\Omega_i. \quad (3)$$

An important implication of such boundary condition is that each immobile region is connected only to the mobile region, i.e. the immobile regions are not connected.

Next step requires to smooth the concentration field applying a suitable spatial filtering. In [29] two filters were defined, the volume filter over the Ω and the Favre filter acting on the volume of the mobile region Ω_m . We will call \bar{c}_m the volume averaged concentration field and \tilde{c}_m the Favre averaged concentration field. The relation between the two is [29]:

$$\bar{c}_m = \beta_m \tilde{c}_m \quad (4)$$

which allows to write the concentration field in terms of a quantity (the Favre filtered concentration field) specific only to the mobile region. In the previous equation we also introduced the capacity of the mobile region, β_m , defined as the ratio between the volume of the region Ω , V , and the volume of the mobile region, V_m $\beta_m = V/V_m$.

By applying the volume filtering to eq. (3) and using eq. (4) along with the Gauss-Green theorem, we obtain the following equation for the filtered quantities:

$$\beta_m \frac{\partial \tilde{c}_m}{\partial t} + \sum_{i=1}^{N_i} \dot{\mathcal{M}}_i(t) = -\nabla \cdot \mathbf{J}_m, \quad (5)$$

where we introduced the average inter-region mass exchange rate for region i , $\dot{\mathcal{M}}_i(t)$, defined as:

$$\dot{\mathcal{M}}_i(t) = \frac{1}{V} \int_{\partial\Omega_i} \mathcal{D}_i \frac{\partial c_i}{\partial n} dS \quad (6)$$

and the total average flux in the mobile region, \mathbf{J}_m . However, following [29] we replace this quantity with the effective flux in the mobile region, $\mathbf{J}_{m,\text{eff}}$, defined as:

$$\mathbf{J}_m = \mathbf{u}_{\text{eff}} \tilde{c}_m - \mathcal{D}_{m,\text{eff}} \nabla \cdot \tilde{c}_m \quad (7)$$

where \mathbf{u}_{eff} and $\mathcal{D}_{m,\text{eff}}$ are the effective velocity and the effective diffusivity, which include the contribution of the capacity β_m . By using the Favre averaged concentration in the immobile region, \tilde{c}_i we can write eq. (1) as:

$$\frac{\partial \tilde{c}_i}{\partial t} = \frac{\dot{\mathcal{M}}_i(t)}{\beta_i} \quad (8)$$

where $\beta_i = V_i/V$ is the capacity of the immobile region i , finally obtaining the multicontinuum equation for the concentration field in the mobile region:

$$\beta_m \frac{\partial \tilde{c}_m}{\partial t} + \sum_{i=1}^{N_i} \frac{\partial \tilde{c}_i}{\partial t} = -\nabla \cdot \mathbf{J}_{m,\text{eff}}, \quad (9)$$

Using the assumption of linearity within each cell and using the subscripts c and f to indicate fields evaluated at the cell and face center respectively, one obtain the discretised system:

$$\left\{ \begin{array}{l} \beta_{m,c} \frac{\partial c_{m,c}}{\partial t} + \sum_{i=1}^{N_i} \sum_{k=1}^{\infty} \beta_{ik,c} \frac{\partial c_{ik,c}}{\partial t} = \frac{1}{V_c} \sum_{f=0}^{N_{c,f}} (\mathcal{D}_{m,f} (\nabla c_m)_f - \mathbf{u}_f c_{m,f}) \cdot \mathbf{n}_{c,f} S_{c,f} \\ \frac{\partial c_{ik,c}}{\partial t} - \lambda_{ik,c} (c_{ik,c} - c_{m,c}) = 0, \quad \begin{array}{l} i = 1, \dots, N_i \\ k = 1, \dots, \infty \\ c = 0, \dots, N_c \end{array} \end{array} \right. \quad (14)$$

Furthermore, the method requires the definition of appropriate discretisation operators to express face-based variables like $(\nabla c_m)_f$ and $c_{m,f}$ as cell-based variables (e.g., $c_{m,c}$). A number of such discretisation methods (e.g., Gauss integration based linear and upwind schemes) are available in OpenFOAM[®] and they will not be discussed here since their effectiveness depends on the specific problem to solve. Unlike previous works [35], the equations for the immobile regions are discretised in time and solved separately and iteratively rather than being included in the equation for the mobile region. While this leads to larger memory requirements and requires a more complex software architecture [35], it also results in a more flexible code. Most importantly, it allows to include more complex transfer models in the future and to couple the equations in an implicit manner through multiple iterations.

3.2 Library structure

The *multiContinuumModels* library follows a flexible object oriented structure. This allows to easily implement new functionalities with relative ease.

A base abstract class named *multiContinuumModel* store references to concentration c_m and capacity β_m in the mobile region, and provides public functions for calculating the source term $\dot{\mathcal{M}}$ as well as for updating the model describing the immobile regions. These are the only functions that need to be called inside an OpenFOAM[®] application to make use of this library.

The *multiContinuumModel* class is base for the *multiRateMassTransfer* class, which holds a list of pointers to *immobileRegion* objects (representing the transfer models for each immobile region) and stores the total concentration in the immobile regions $\sum_i c_i$. This class also implements the function that returns the overall source term $\dot{\mathcal{M}}$.

Classes derived from the *immobileRegion* abstract class are at the core of the multi-rate model, since they implement different kind of transfer models based on the geometrical and physical properties of the medium. Each immobile region holds a list of pointers to fields representing the concentration c_{ik} corresponding to each term in the multi-rate series. The length of such array is given by the *nOfTerms* label, and is read at the beginning of the simulation. Furthermore, this class stores the concentration in the immobile region c_i , the relative capacity β_i , and the frequency ω_i . These are all fields, and can be defined by the user as uniform or non-uniform (e.g., non-uniform initial condition on c_i , spatially varying capacity β_i and medium properties ω_i). This class also implements a function that solves the system of ODEs for the multi-rate terms. The multi-rate coefficients α_{ik} and β_{ik} are computed in derived classes, specialized for spheres, layers, cylinders, and first order reactions.

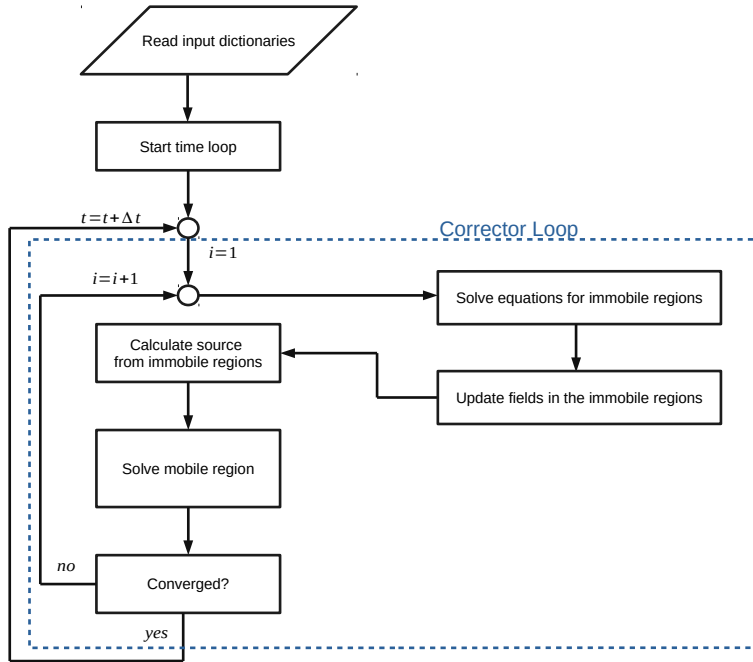


Figure 2: Diagram showing the numerical algorithm for *mrmtScalarTransportFoam*.

3.3 *mrmtScalarTransportFoam*

The library includes an application for solving the scalar transport equations with the multi-rate mass transfer model. Such application, named *mrmtScalarTransportFoam*, solves the system of equations 14, corresponding to the multi-rate model of Haggerty and Gorelick [20]. The solver is based on the standard *scalarTransportFoam* available in native OpenFOAM[®] and employs a special *multiContinuumControl* object (derived from the PIMPLE algorithm in OpenFOAM[®]) that wraps the *multiContinuumModel* library and checks for convergence.

The complete solution algorithm (including operations performed by the *multiContinuumModel* library) is illustrated in Figure 2, and it consists in a time loop with a nested corrector loop possessing a sub-time stepping loop. These operations can be summarised as follows:

- **Corrector loop:** this is the principal solution step. It consists in solving the governing equations for the immobile regions (with the optional sub-time stepping) and the advection-diffusion equation for the mobile region sequentially, in a segregated manner. When the residuals fall below a certain threshold or the maximum number of iterations (defined by the user) has been reached, the solver exits the loop.
- **Time loop:** it constitutes the main loop. After a satisfactory solution has been achieved in the corrector loop, the algorithm moves on to the next time step.

3.4 Input files

Input data and controls are provided by mean of appropriate 'dictionaries' (i.e., input files in OpenFOAM[®] terminology). In the *multiContinuumModel* library, input parameters must be provided in the *multiRateProperties* dictionary located in the folder *constant* (see the OpenFOAM[®] [33] details regarding the structure of simulation folders).

3.4.1 multiRateProperties dictionary

Listing 1 shows an example of basic input for the *multiRateProperties* dictionary. The first lines (1 to 8) are the required OpenFOAM[®] header, and are present in all dictionaries in a similar fashion. Lines 11 and 12 control the time-step adaptivity. In fact, the library allows to automatically set the time step Δt in such way that the reaction-based Courant number satisfies:

$$Co_\lambda = \max(\alpha_{ik}\omega) \Delta t < Co_{\max}, \quad (15)$$

where Co_{\max} is the read from line 12. Ensuring that $Co_\lambda < 1$ is a necessary condition to obtain accurate and bounded results and therefore it is highly advised to keep this option active. However, in many applications (as groundwater transport) the time scale corresponding to the transport in the mobile region will be much smaller than the time scale of the mobile-immobile transfer. Therefore, in most circumstances the time step will not need to be adjusted.

Lines 14 to 24 of listing 1 contain the list of immobile regions. Each region is specified as a sub-dictionary with a user-defined name, which will be used by the library to identify the region and build the appropriate fields. Lines 16 to 23 show one immobile region as example. All immobile regions have the following entries:

- `type`: this is the type of immobile region, which defines how the α_{ik} and β_{ik} are computed.
- `numberOfTermsInExpansion`: defines how many terms should be retained in the expansion.
- `rescaleBetas`: this entry allows to decide how the truncation of the series is handled. If set to true, all β_{ik} are rescaled such that $\sum_k \beta_{ik} = 1$ as in [35]. By default, this entry is set to false and a 'truncation capacity' $\beta_{tr} = 1 - \sum_k \beta_{ik} \neq 0$ will be computed. This truncation capacity will then be added to the capacity of the mobile region, as if the truncated terms were in equilibrium with the mobile concentration [29].

```
1 FoamFile
2 {
3     version      2.0;
4     format       ascii;
5     class        dictionary;
6     location     "constant";
7     object       multiRateProperties;
8 }
9
10 //- Controls for time-step adaptivity
11 adaptiveTimeStepping true;
12 maxCo           0.95;
13
14 immobileRegions //- List of immobile regions
15 (
16     nameOfRegion //- This can be any name
17     {
```

Type	α_{ik}	β_{ik}
Layers	$\frac{(2k-1)^2 \pi^2}{4}$	$\frac{8}{(2k-1)^2 \pi^2}$
Cylinders	ζ_k^2	$\frac{4}{\zeta_k^2}$
Spheres	$k^2 \pi^2$	$\frac{6}{k^2 \pi^2}$
FirstOrderReactions	alphaCoeffs	betaCoeffs

Table 1: Expressions for α_{ik} and β_{ik} for different types of immobile regions. Here ζ_k corresponds to the k -th zero of the 0-Bessel function of the first kind. The eigenvalues λ_{ik} can be obtained using eq. (12) and the α^* reported in tables 2 and 3

```

18     // - Type of immobile region
19     type                Spheres;
20
21     // - Terms to represent the immobile region
22     numberOfTermsInExpansion    50;
23
24     // - How the truncation is handled
25     rescaleBetas                false;
26 }
27 );

```

Listing 1: Basic input for the *multiRateProperties* dictionary

3.4.2 Immobile regions

At the current stage, there are four different immobile region types available: Spheres, Cylinders, Layers, and first-order reactions. Table 1 shows how the values of α_{ik} and β_{ik} are computed for different immobile regions. Since the zeros of the Bessel function are not computed explicitly, but are stored in an array, cylindrical immobile regions are limited to 20 terms in the expansion. First-order reactions are the most flexible kind of immobile region, since the values of α_{ik} and β_{ik} are read directly from the dictionary. This makes the such immobile region appropriate for calibration studies.

Listing 2 shows the syntax for a first-order reaction region. Notice that the number of entries in `alphaCoeffs` and `betaCoeffs` must be equal to `numberOfTermsInExpansion`.

```

1     immobile
2     {
3
4         type                FirstOrderReactions;
5         numberOfTermsInExpansion    3;
6         alphaCoeffs         nonuniform (1 2 3);
7         betaCoeffs          nonuniform (0.5 0.3 0.2);
8     }

```

Listing 2: Example of a FirstOrderReactions immobile region (named 'immobile') with three terms

In addition to being defined in *multiRateProperties*, immobile regions require a set of fields representing the initial condition, the capacity, and the transfer rate. These fields can be summarised (for each immobile region) as:

- `c.[name of region]`: is the field representing the field c (concentration) in that immobile region. It is possible to specify an initial condition for this field following the standard OpenFOAM[®] syntax [33].
- `omega.[name of region]`: is the field representing the transfer rate for that immobile region. This field represents the material properties related to a immobile region and can vary in space and time. Specifically, it coincides with the ration between the diffusion coefficient and the square of a reference length for all region types except FirstOrderReactions.
- `beta.[name of the region]`: represents the capacity of the immobile region, and can vary in space and time.

The *tutorials* folder in the library provides a range of examples illustrating the syntax and how to structure a simulation folder.

4 Results and discussion

In this Section we show different application of our library in different situations taken from problems in heterogeneous geological media and flow in packed bed equipment. We choose the different systems mainly to show the the flexibility of our model and implementation in different situations, but they also have the purpose to show the wide range of applicability of such a model. We start from a simple 0D model and then we move to more realistic-like cases in following sections.

We will also present some results in terms of different number of expansions, which will be indicated as M (i.e. we truncate at M the innermost sum in eq. (14)). The truncation is handled through *rescaleBetas*, which is described in section 3.4.1.

4.1 Zero-dimensional test-case

For the zero-dimensional test-case, we solve eq. (13) in OpenFOAM[®] in a domain composed by a single cell. In this way, we obtain a situation similar to the one described in Haggerty and Gorelick [20] for a batch reactor (no advection, dispersion, sources and sinks). We choose to represents the immobile zone as composed by seven spherical immobile regions, and we called this the 7Sp model. This in analogue to the one reported in Tab.2 of Haggerty and Gorelick [20], with the same β and ω which we report in table 2. Our purpose here is to compare the results with a known solution to show the accuracy of our implementation.

We report the results for four expansions, identified by $M = 2, 10, 20, 50$, in terms of the normalized concentration of the mobile zone \tilde{c}_m , defined as

$$\tilde{c}_m = \frac{c_{eq} - c_m(t)}{c_{eq} - c_{m,in}}, \quad (16)$$

	α_i^* (s ⁻¹)	β_i
Sphere1	$3.1 \cdot 10^{-8}$	0.0406
Sphere2	$9.2 \cdot 10^{-8}$	0.1699
Sphere3	$2.3 \cdot 10^{-7}$	0.2731
Sphere4	$2.7 \cdot 10^{-7}$	0.2592
Sphere5	$9.4 \cdot 10^{-7}$	0.1548
Sphere6	$1.7 \cdot 10^{-6}$	0.0620
Sphere7	$1.4 \cdot 10^{-6}$	0.0404

Table 2: Values of α_i^* (where $i = 1, \dots, 7$) and capacity coefficients β_i as reported in Tab.2 of Haggerty and Gorelick [20] used for the calculation of the 7Sp model.

where c_{eq} equilibrium concentration between mobile and immobile zones, $c_{m,in}$ initial concentration in the mobile zones, $c_m(t)$ concentration in the mobile zone at time t . The curve we obtain is shown in fig. 3. As it can be seen, using only two expansion (i.e. $M = 2$) is not sufficient to capture the dynamics of the process. However, $M = 10$ seems already enough to obtain good quantitatively agreement with known results (see Figure 2-b in [20]). As expected, the agreement increases as we increase the number of expansions. However, notice that our method is prescribing a slightly different trend due to the method used to account for the truncated terms, which is not present in [20].

4.2 One-dimensional test-case

In order to assess the accuracy of our numerical method and the correct implementation of the library, we compare results from the `mrmtScalarTransportFoam` numerical solver described in section 3.3 against a spectral solution for a simple problem. We therefore consider the following system of equations:

$$\begin{cases} \frac{\partial c_m}{\partial t} + \frac{\partial c_m}{\partial x} - \frac{1}{10} \frac{\partial^2 c_m}{\partial x^2} = \frac{1}{2} (c_i - c_m) \\ \frac{\partial c_i}{\partial t} = (c_m - c_i). \end{cases} \quad (17)$$

Together with the following boundary conditions:

$$\left. \frac{\partial c_i}{\partial x} \right|_{x=0} = \left. \frac{\partial c_i}{\partial x} \right|_{x=1} = 0, \quad c_m(t, 0) = 0, \quad \left. \frac{\partial c_m}{\partial x} \right|_{x=1} = 0, \quad (18)$$

and initial conditions:

$$c_m(0, x) = 0, \quad c_i(0, x) = 1. \quad (19)$$

Notice that the coefficients appearing in system 17 are chosen arbitrarily to generate fast transients dominated by convection and reaction, and do not necessarily represent any realistic application to groundwater flows. However, they provide an excellent test for the numerical stability of this algorithm.

In this simplified mathematical model, at time $t = 0$ mobile and immobile regions begin exchanging mass, starting from a condition of non-equilibrium. Specifically, mass is transferred from the

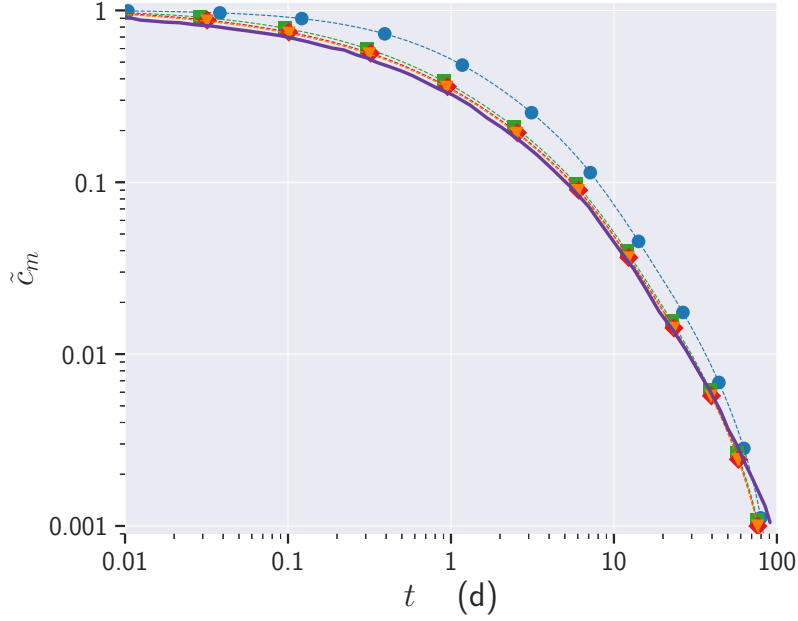


Figure 3: Breakthrough curves at different expansion for the 7Sp model (see table 2) compared with the same model reported in Haggerty and Gorelick [20]. Purple continuous curve is taken from [20] (Table 2), blue \bullet $M=2$, green \blacksquare $M = 10$, red \blacklozenge $M = 20$, orange \blacktriangledown $M = 50$

immobile region to the mobile region and then transported out of the domain by advection. System 17 is solved using the Matlab-based library Chebfun [14], which employs Chebyshev polynomials to solve systems of differential equations to spectral accuracy, providing our benchmark solution. System 17 is discretized in OpenFOAM[®] using of second order schemes in space (i.e., linear upwind and central differences) and in time (backward). A grid of 20 cells was employed and the time step was chosen to satisfy the Courant-Friedrichs-Lewys condition $Co = U\Delta t/\Delta x < 1$ [11], where Co is the Courant number, $U = 1$, Δt is the time step, and Δx is the mesh spacing. Figure 4 shows excellent agreement between the breakthrough curve predicted by Chebfun and that predicted by `mrmtScalarTransportFoam`. We notice in passing that our solver required a smaller (by a factor of ten) time step to match the solution of Chebfun. This is due to the limited (second order) accuracy of OpenFOAM[®] compared to the spectral representation in Chebfun.

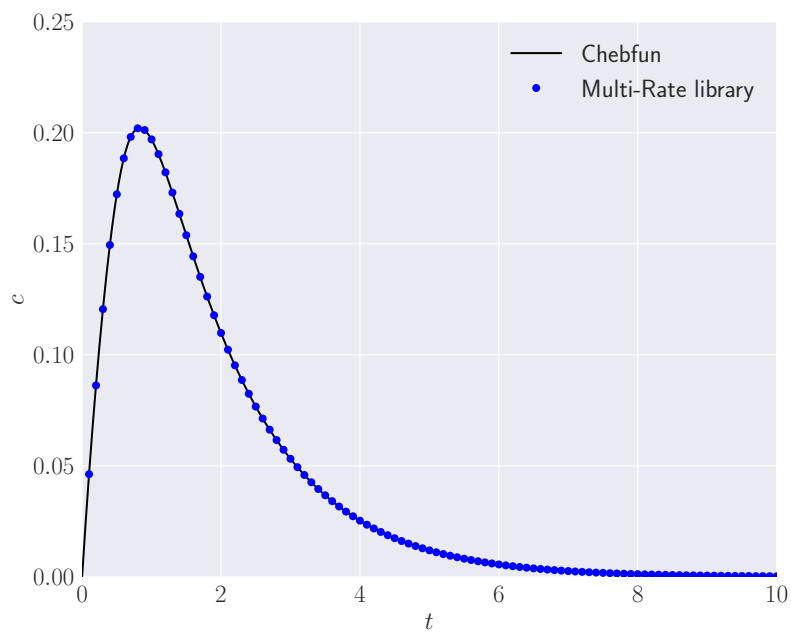


Figure 4: Breakthrough curves from Chebfun [14] and `mrmtScalarTransportFoam`

4.3 Two-dimensional simulation of heterogeneous geological media

In this section we will report some application of the `mrmtScalarTransportFoam` in different conditions which represent different physical applications. Our computational domain is a 2D domain of width 2m and height 1m, numerical grid was built in OpenFOAM® using the `blockmesh` utility, which allows the generation of orthogonal hexahedral meshes. The total number of cell in our computational domain is 20000.

In all the cases considered, the flow field was generated using the same algorithm, which we are going to describe in his general outlines here, with different initial conditions, specific for each case which will be analysed in each relevant section.

The flow field in our porous media is obtained by solving the steady-state Darcy equation:

$$\frac{K}{\mu} \nabla P = \mathbf{u} \quad (20)$$

$$\nabla \cdot \mathbf{u} = 0 \quad (21)$$

where μ is the dynamic viscosity of the fluid, K is the tensor permeability field, and the boundary conditions on the pressure represent the ΔP on the two ends of the computational domain. From eq. (20) we can obtained a Poisson equation whose resolution is implemented in a new OpenFOAM® solver, `simpleDarcyFoam`, which solves for the Darcy pressure in general grids. The permeability field can be constant in the domain, generated randomly according to some statistics or obtained from measurements. The velocity and the pressure are coupled using a SIMPLE loop, which is also used for non-orthogonal grid corrections and to couple the deviatoric part of the permeability tensor field.

4.3.1 Solute transport in geological media

Solute transport in geological media have received considerable attention in literature, because their connection with the study of dispersion of contaminants [27, 38, 12].

Geological media main feature is heterogeneity, and we recover this feature employing random permeability field, which is shown in fig. 5a. One thing to notice is the magnitude of the permeability around 1 m^2 which is several order of magnitude higher than one encountered in practice. This does not constitute an issue, as long as we use a pressure drop which returns a velocity field consisted with the ones observed in geological media (laminar regime and velocity of the order of 0.1 m^2). We solve eq. (20) with a pressure drop of $\Delta P = 10^{-6}$ (which translates to Dirichlet boundary conditions of $P(0, z) = 10^{-6}$ and $P(L, z) = 0$). As expected, the higher velocities corresponds to regions with higher permeability K .

For this case we will consider three different models: *i*) the 7Sp model that we discussed in section 4.1 (see also table 2), *ii*) the *Composite* (Comp) model summarised in table 3 and, *iii*) the *Random* (Rand2D) model, with one immobile spherical region for which all the relevant parameters K , β_i , and α_i^* are non-uniform and generated randomly in the domain.

We will mainly focus our discussion on the 7Sp model and at the end of the section we will show some results for the Comp and Rand2D model.

One of the quantity which is of interest in these kind of calculations, is the flowing of the concentration of the contaminant flowing out of the domain. The results for the 7Sp model are reported in fig. 6. Here, we only show the curve at $M = 2$ since they are all very similar at the scale of the plot.

In this case the normalized concentration of the mobile zone \tilde{c}_m , is defined as:

$$\tilde{c}_m(t) = \frac{c_m(t)}{c_m(0)}, \quad (22)$$

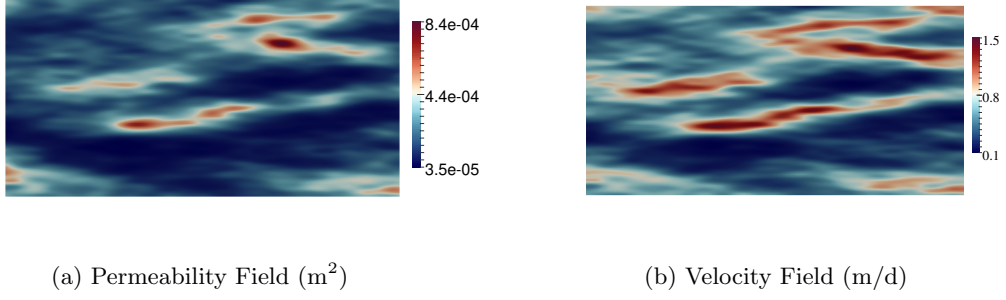


Figure 5: Contour plot of the randomly generated Permeability Field and the corresponding Velocity Field obtained by solving eq. (20)

	α_i^* (s ⁻¹)	β_i
Sphere1	$2.8 \cdot 10^{-7}$	0.35
Sphere2	$1.75 \cdot 10^{-8}$	0.20
Layer1	$1.43 \cdot 10^{-9}$	0.15
Cylinder1	$1.00 \cdot 10^{-9}$	0.15
Reaction1	$2.76 \cdot 10^{-6}$	0.05
Reaction2	$4.42 \cdot 10^{-5}$	0.10

Table 3: Values of α_i^* (where $i = 1, \dots, 7$) and capacity coefficients β_i as reported in Tab.3 of Haggerty and Gorelick [20] used for the calculation of the Comp model.

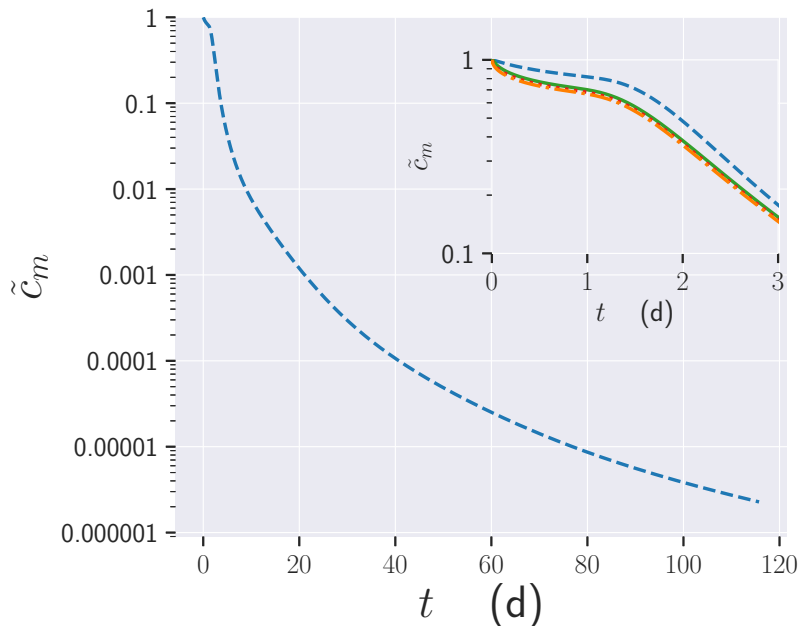


Figure 6: Breakthrough curves for the 7Sp case and $M = 2$. In the inset, are reported the results for the first 3 days for all the expansion considered: $M = 2$ dashed blue curve, $M = 10$ green continuous curve, $M = 20$ dotted curve, $M = 50$ dash-dotted curve

where $c_m(0)$ is the concentration in the mobile zone at time $t = 0$. In this case we considered the immobile regions empty (i.e. $c_{im} = 0$) and the mobile region with some contaminant $c_m > 0$.

One thing to notice is the change in the slope at the very beginning of the curve, which is reported in more detail in the inset in fig. 6 for all the different expansion. This variation is due to the fact that we started from a non-equilibrium situation, where the immobile regions are completely empty and the beginning of the simulation is dominated by the exchange between mobile and immobile regions. Here, we can also see some of the differences given by a model with different number of expansions. For $M > 10$ the results completely agree and the dynamic described is much faster than the one obtained with two modes only. That is because two modes is not enough to capture all the relevant characteristic times of the system, on the other hand, ten modes are enough to capture all the relevant behaviours of this system.

The rapid exchange of contaminant between the mobile and immobile regions is qualitatively shown in figs. 7 and 8 where the contour plots at different times of the variation of the mobile components (fig. 7) and immobile one (fig. 8) in the 2D domain are reported. As can be observed, the process is nearly completed after approximately one day. A more quantitative results of the time variation of the contaminant into the immobile region is reported in fig. 9, where the process of accumulation of the contaminant following by its discharge can be observed for three different immobile regions.

The Comp model gives results similar to the one presented for the 7Sp model, they are summarised in fig. 10. We can still observe a transient at the beginning of the simulation, which however, results much faster than the one shown in the 7Sp model (see fig. 6).

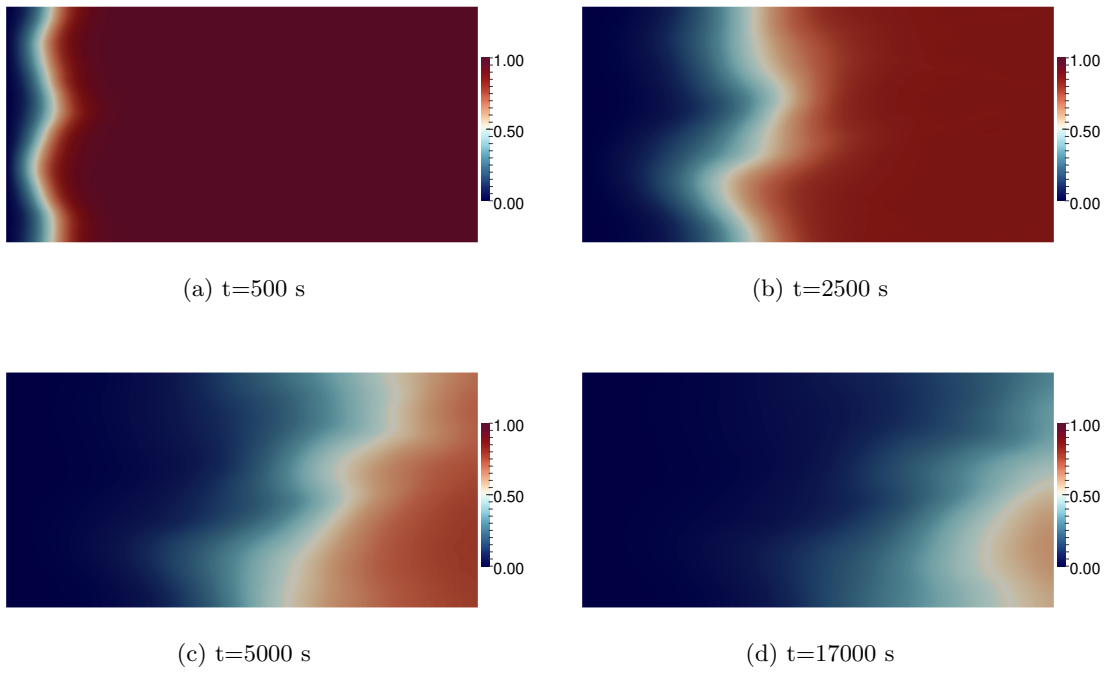


Figure 7: Contour plot of the concentration of the contaminant in the mobile zone (kg/m^3)

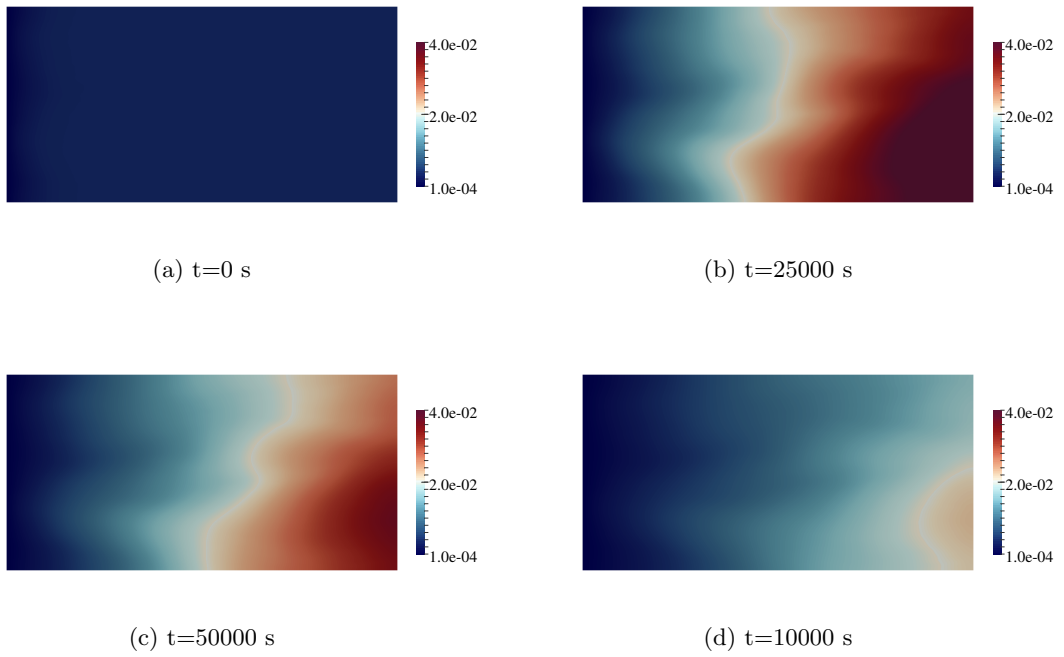


Figure 8: Contour plot of the concentration in (kg/m^3) of the contaminant in the immobile zone (sphere1 as defined in table 2) for the Sphere1 (see table 2)

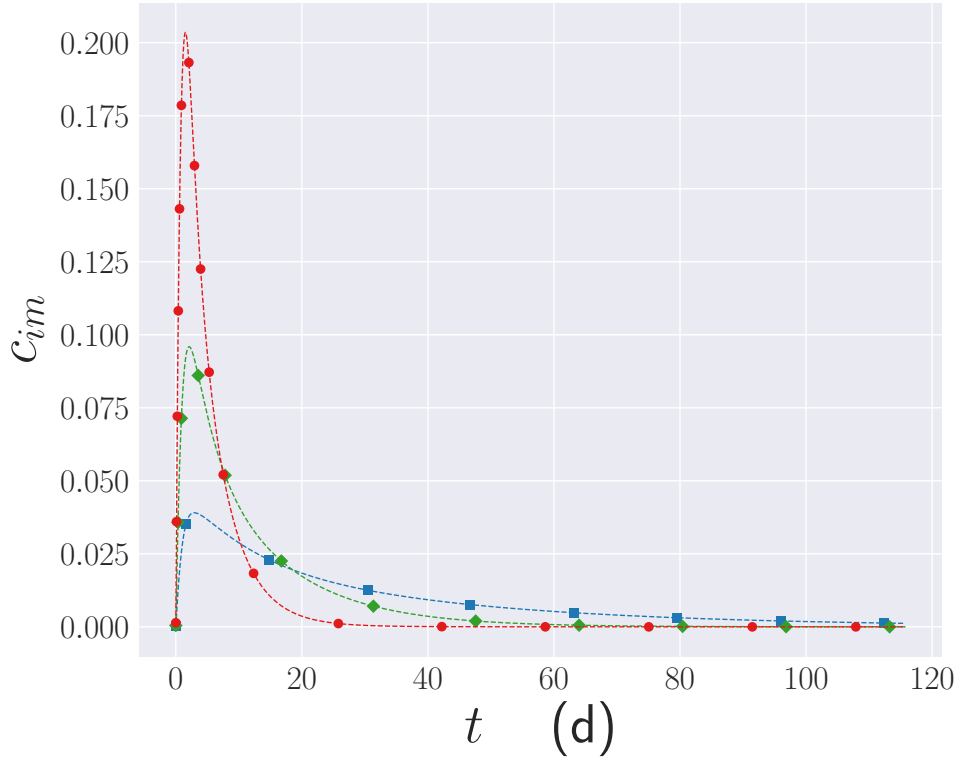


Figure 9: Concentration of the contaminant versus time in three of the immobile zones in the Sp7 model. Sphere2: red • $M = 10$, Sphere3: green ■, Sphere5 blue ◆

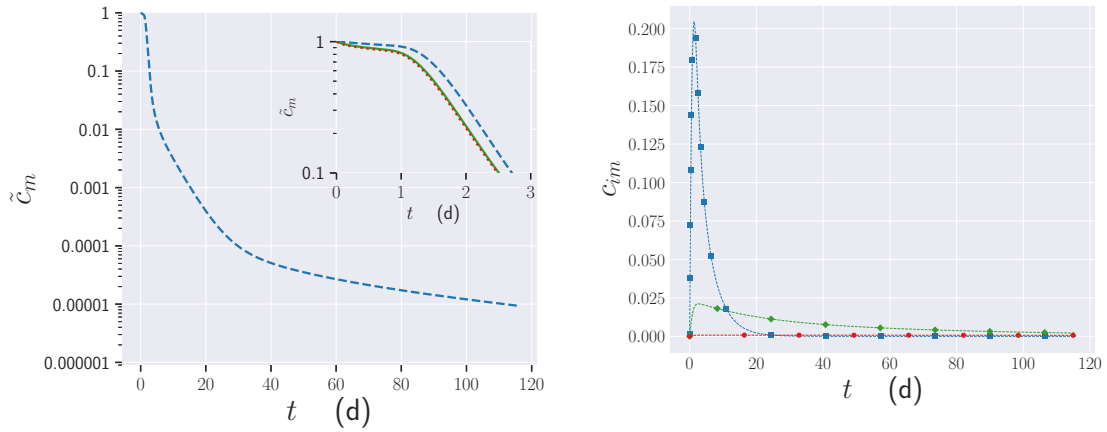


Figure 10: On the left: Breakthrough curves for the 7Sp case and $M = 2$. In the inset, are reported the results for the first 3 days for all the expansion considered: $M = 2$ dashed blue curve, $M = 10$ green continuous curve, $M = 20$ dotted curve, $M = 50$ dash-dotted curve. On the right: Concentration of the contaminant cm (in kg/m^2) versus time in three of the immobile zones in the Comp model. Sphere2: red • $M = 10$, Cylinder1: green ■, Reaction1 blue ◆

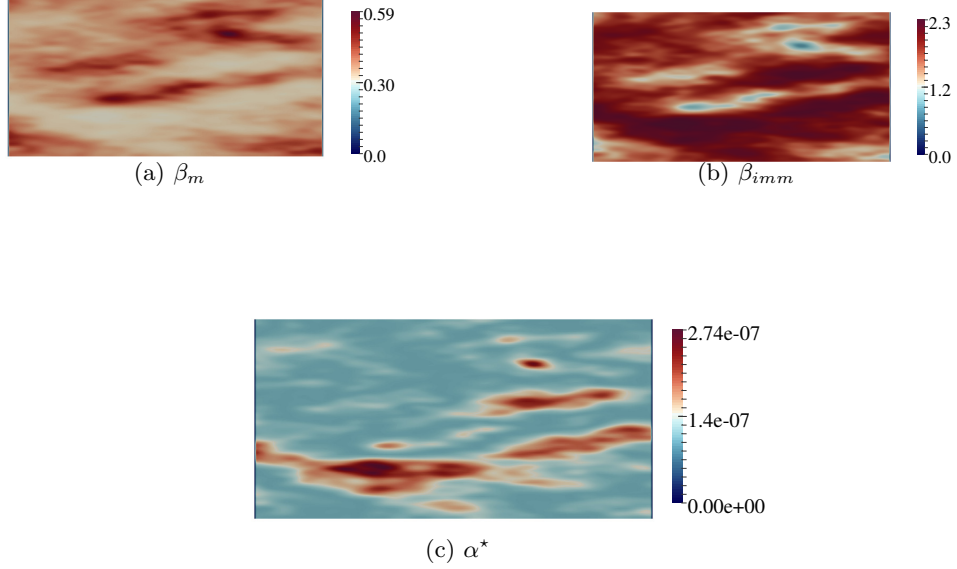


Figure 11: Contour plot of the fields for β , β_{imm} and α^* generated using eq. (23)

4.3.2 Random Case

The last case we consider for multi rate process in geological media is the one in which all the relevant parameters (K , α and β) are random. For this case, we consider only one immobile region modelled as sphere, we call this case R1Sp.

We start by building the β_m field which we choose to have some correlation with K . To this end, we map the permeability random field K shown in fig. 5a into a field for β_m by associating to each K a value in $[0.3, 0.6]$. The final field for β_m is shown in section 4.3.2. From β_m , using the Kozeny-Carman law we obtain for β_{im} and ω :

$$\alpha^* = a \frac{\beta_m^3}{K(1 - \beta_m)^2} \quad (23)$$

$$\beta_{im} = \frac{1 - \beta_m}{\beta_m}$$

where $a = 10^{-10}$, which are shown in section 4.3.2 and fig. 11c.

Results, in terms of the concentration of the contaminant leaving the domain, and the load-unload cycle of the immobile region are reported in fig. 12. We can observe the same transient at the very beginning of our simulation, as already shown before (see figs. 6 and 10)

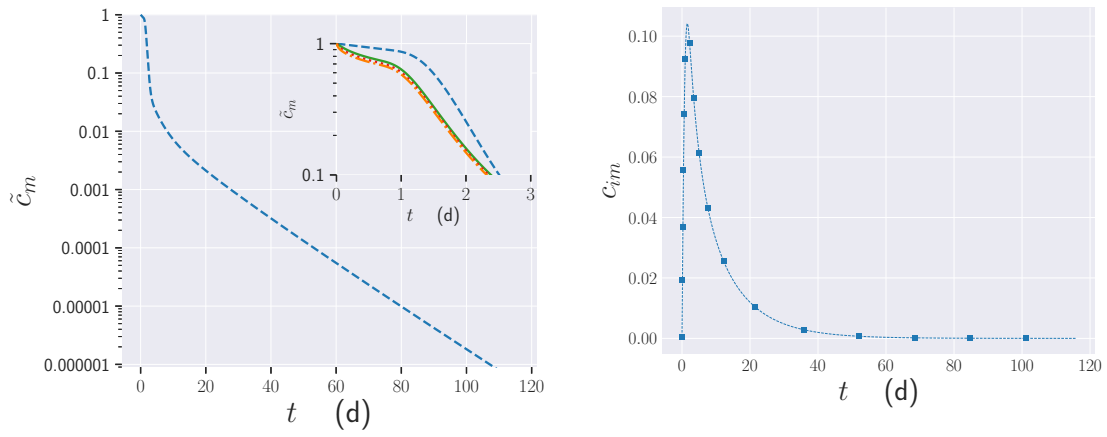


Figure 12: On the left: Breakthrough curves for the R1Sp case and $M = 2$. In the inset, are reported the results for the first 3 days for all the expansion considered: $M = 2$ dashed blue curve, $M = 10$ green continuous curve, $M = 20$ dotted curve, $M = 50$ dash-dotted curve. On the right: Concentration of the contaminant cm (in kg/m^2) versus time in the immobile region

4.4 Three-dimensional packed bed

Packed bed reactors occupy a predominant role in chemical industry [25], where they are used in several different processes such as separation, filtration, purification or as a reaction unit and their modelling at different level and scales [19, 8, 24] which can also include the modelling of the reactions inside the domains [9]. The flow field and transport phenomena (like heat and mass transfer) inside these equipment can be described different level of resolution, as pseudo-homogenous models which consider a single phase, or particle-resolved models, where the components of the packing material (such as spheres) are fully described [25, 7].

In this work we will follow the first route and we will describe the flow field inside the packed bed reactor as we did in the previous section (see section 4.3), by solving the steady-state Darcy equation eq. (20) on a randomly generated permeability field.

The domain is represented by a 3D cylinder with height 0.5 m and base diameter of 0.06 m. The mesh is composed by 64000 cells.

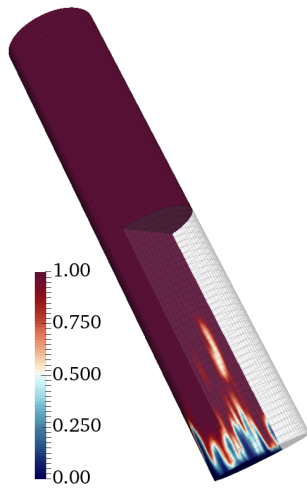
The simulation setup is summarized here:

- `div(phi,c)` bounded Gauss vanLeer01[39];
- `gradSchemes`: `cellLimited leastSquares 1`;
- `snGradSchemes`: `default limited 1`;

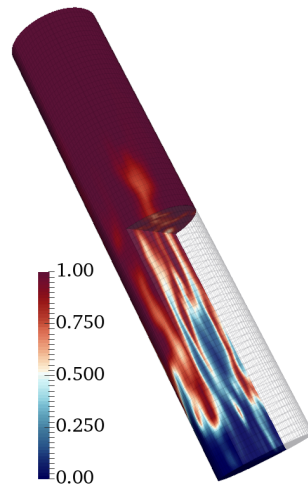
The numerical solution scheme used unsure that the concentration of the chemical species inside the packed bed remains bounded to the initial value.

The permeability and the flow field inside the domain were generated as described in the previous section by solving the steady-state Darcy equation (see eq. (20)). We used for this system the 7Sp model described earlier (see table 2).

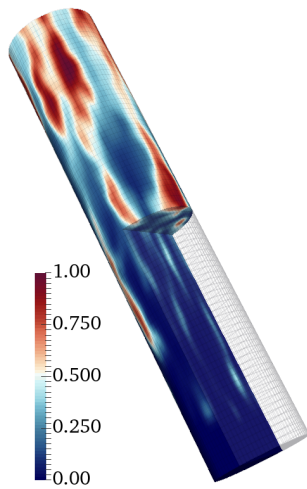
In fig. 13 we show the variation of the chemical species inside the reactor in the mobile region at different times.



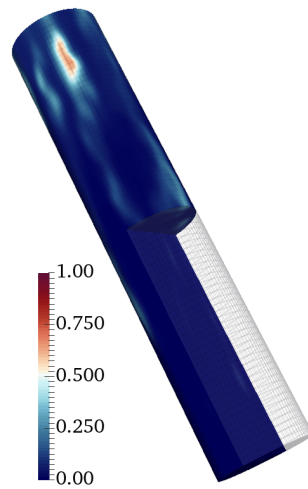
(a) $t=2$ s



(b) $t=20$ s



(c) $t=40$ s



(d) $t=80$ s

Figure 13: Contour plot of the concentration of the chemical species in (kg/m^3) in the mobile zone for the Packed Bed reactor at different times

5 Conclusions

In this work, we presented an OpenFOAM[®] library to solve problems involving non-local (in time) transport phenomena using the Multi-Rate Mass Transfer model first proposed in Haggerty and Gorelick [20] and subsequently formalized in Municchi and Icardi [29]. We showed that the numerical solver included in the library produces results in agreement with previous works and Chebfun [14] calculations, and we proposed a number of cases that illustrate possible applications to chemical engineering and geological media.

Acknowledgements

This work has been funded by the European Union’s Horizon 2020 research and innovation programme, grant agreement number 764531, ”SECURE – Subsurface Evaluation of Carbon capture and storage and Unconventional risks”.

References

- [1] A. Adeyemo, R. Kumar, P. Linga, J. Ripmeester, and P. Englezos. Capture of carbon dioxide from flue or fuel gas mixtures by clathrate crystallization in a silica gel column. *International Journal of Greenhouse Gas Control*, 4(3):478–485, 2010.
- [2] D. A. Benson and M. M. Meerschaert. A simple and efficient random walk solution of multi-rate mobile/immobile mass transport equations. *Advances in Water Resources*, 32(4):532–539, 2009.
- [3] B. Berkowitz and H. Scher. Theory of anomalous chemical transport in random fracture networks. *Physical Review E*, 57(5):5858, 1998.
- [4] B. Berkowitz and H. Scher. Exploring the nature of non-fickian transport in laboratory experiments. *Advances in Water Resources*, 32(5):750–755, 2009.
- [5] B. Berkowitz, A. Cortis, M. Dentz, and H. Scher. Modeling non-Fickian transport in geological formations as a continuous time random walk. *Reviews of Geophysics*, 44(2), 2006.
- [6] B. Berkowitz, S. Emmanuel, and H. Scher. Non-Fickian transport and multiple-rate mass transfer in porous media. *Water Resources Research*, 44(3), 2008.
- [7] G. Boccardo, F. Augier, Y. Haroun, D. Ferre, and D. L. Marchisio. Validation of a novel open-source work-flow for the simulation of packed-bed reactors. *Chemical Engineering Journal*, 279: 809–820, 2015.
- [8] G. Boccardo, R. Sethi, and D. L. Marchisio. Fine and ultrafine particle deposition in packed-bed catalytic reactors. *Chemical Engineering Science*, 198:290–304, 2019.
- [9] Gianluca Boccardo, Igor M Sokolov, and Amir Paster. An improved scheme for a robin boundary condition in discrete-time random walk algorithms. *Journal of Computational Physics*, 374: 1152–1165, 2018.
- [10] J. Carrera, X. Sánchez-Vila, I. Benet, A. Medina, G. Galarza, and J. Guimerà. On matrix diffusion: formulations, solution methods and qualitative effects. *Hydrogeology Journal*, 6(1): 178–190, 1998.

- [11] R. Courant, K. Friedrichs, and H. Lewy. Über die partiellen Differenzgleichungen der mathematischen Physik. *Mathematische Annalen*, 100(1):32–74, dec 1928. ISSN 0025-5831. doi: 10.1007/BF01448839. URL <http://link.springer.com/10.1007/BF01448839>.
- [12] E Crevacore, G Boccardo, D Marchisio, and Rajandrea Sethi. Microscale colloidal transport simulations for groundwater remediation. *Chemical Engineering Transactions*, 47:271–276, 2016.
- [13] M. Dentz, A. Cortis, H. Scher, and B. Berkowitz. Time behavior of solute transport in heterogeneous media: transition from anomalous to normal transport. *Advances in Water Resources*, 27(2):155–173, 2004.
- [14] T. A Driscoll, N. Hale, and L. N. Trefethen. *Chebfun Guide*. Pafnuty Publications, 2014. URL <http://www.chebfun.org/docs/guide/>.
- [15] The Openfoam Foundation. The OpenFOAM Foundation. pages 4–5, 2014.
- [16] S. Geiger, M. Dentz, and I. Neuweiler. A Novel Multi-rate Dual-porosity Model for Improved Simulation of Fractured and Multi-porosity Reservoirs. *SPE Reservoir Characterization and Simulation Conference and Exhibition*, (August), 2011. ISSN 1086-055X. doi: 10.2118/148130-MS. URL <http://www.onepetro.org/doi/10.2118/148130-MS>.
- [17] A. Georgi, A. Schierz, K. Mackenzie, and F. Kopinke. Colloidal activated carbon for in-situ groundwater remediation—Transport characteristics and adsorption of organic compounds in water-saturated sediment columns. *Journal of contaminant hydrology*, 179:76–88, 2015.
- [18] P. Gouze, Y. Melean, T. Le Borgne, M. Dentz, and J. Carrera. Non-Fickian dispersion in porous media explained by heterogeneous microscale matrix diffusion. *Water Resources Research*, 44(11), 2008.
- [19] Zehua Guo, Zhongning Sun, Nan Zhang, Ming Ding, and Shuai Shi. Cfd analysis of fluid flow and particle-to-fluid heat transfer in packed bed with radial layered configuration. *Chemical Engineering Science*, 197:357–370, 2019.
- [20] R. Haggerty and S. M. Gorelick. Multiple-Rate Mass Transfer for Modeling Diffusion and Surface Reactions in Media with Pore-Scale Heterogeneity. *Water Resources Research*, 31(10): 2383–2400, oct 1995. ISSN 00431397. doi: 10.1029/95WR10583. URL <http://doi.wiley.com/10.1029/95WR10583>.
- [21] R. Haggerty, S. A McKenna, and L. C. Meigs. On the late-time behavior of tracer test breakthrough curves. *Water Resources Research*, 36(12):3467–3479, 2000.
- [22] I. Herrera and L. Rodarte. Integrodifferential equations for systems of leaky aquifers and applications: 1. The nature of approximate theories. *Water Resources Research*, 9(4):995–1005, 1973.
- [23] I. Herrera and R. Yates. Integrodifferential equations for systems of leaky aquifers and applications 3. A numerical method of unlimited applicability. *Water Resources Research*, 13(4): 725–732, 1977.
- [24] Martin Thomas Horsch, Christoph Niethammer, Gianluca Boccardo, Paola Carbone, Silvia Chiacchiera, Mara Chiricotto, Joshua D Elliott, Vladimir Lobaskin, Philipp Neumann, Peter Schiffels, et al. Semantic interoperability and characterization of data provenance in computational molecular engineering. *Journal of Chemical & Engineering Data*, 2019.

- [25] A Jafari, P Zamankhan, SM Mousavi, and K Pietarinen. Modeling and cfd simulation of flow behavior and dispersivity through randomly packed bed reactors. *Chemical Engineering Journal*, 144(3):476–482, 2008.
- [26] H. Liu, S. Mukhopadhyay, N. Spycher, and B. M. Kennedy. Analytical solutions of tracer transport in fractured rock associated with precipitation-dissolution reactions. *Hydrogeology Journal*, 19(6):1151, 2011.
- [27] R Mackay and TA Cooper. Contaminant transport in heterogeneous porous media: a case study. 1. site characterisation and deterministic modelling. *Journal of hydrology*, 175(1-4): 383–406, 1996.
- [28] Fadl Moukalled, L Mangani, Marwan Darwish, et al. *The finite volume method in computational fluid dynamics*, volume 113. Springer, 2016.
- [29] F. Municchi and M. Icardi. Generalized multirate models for conjugate transfer in heterogeneous materials. *Physical Review Research*, 2(1):013041, 2020.
- [30] Federico Municchi and Matteo Icardi. Generalised Multi-Rate Models for conjugate transfer in heterogeneous materials. *arXiv e-prints*, art. arXiv:1906.01316, Jun 2019.
- [31] I. Neretnieks. Diffusion in the rock matrix: An important factor in radionuclide retardation? *Journal of Geophysical Research: Solid Earth*, 85(B8):4379–4397, 1980.
- [32] S. P. Neuman and D. M. Tartakovsky. Perspective on theories of non-Fickian transport in heterogeneous media. *Advances in Water Resources*, 32(5):670–680, 2009.
- [33] *OpenFOAM: The Open Source CFD Toolbox*. The OpenFOAM Foundation, <https://openfoam.org/>, v1906 edition, 2019.
- [34] K. Roth and W. A. Jury. Linear transport models for adsorbing solutes. *Water resources research*, 29(4):1195–1203, 1993.
- [35] O. Silva, J. Carrera, M. Dentz, S. Kumar, A. Alcolea, and M. Willmann. A general real-time formulation for multi-rate mass transfer problems. *Hydrology and Earth System Sciences*, 13(8):1399–1411, aug 2009. ISSN 1607-7938. doi: 10.5194/hess-13-1399-2009. URL <http://www.hydro1-earth-syst-sci.net/13/1399/2009/>.
- [36] Y. Song, X. Wang, M. Yang, L. Jiang, Y. Liu, B. Dou, J. Zhao, and S. Wang. Study of selected factors affecting hydrate-based carbon dioxide separation from simulated fuel gas in porous media. *Energy & Fuels*, 27(6):3341–3348, 2013.
- [37] E. A. Sudicky and E. O. Frind. Contaminant transport in fractured porous media: Analytical solutions for a system of parallel fractures. *Water Resources Research*, 18(6):1634–1642, 1982.
- [38] DH Tang, EO Frind, and Edward Allan Sudicky. Contaminant transport in fractured porous media: Analytical solution for a single fracture. *Water resources research*, 17(3):555–564, 1981.
- [39] Bram Van Leer. Towards the ultimate conservative difference scheme. ii. monotonicity and conservation combined in a second-order scheme. *Journal of computational physics*, 14(4):361–370, 1974.
- [40] L. Wang, R. D. Vigil, and R. O. Fox. CFD simulation of shear-induced aggreation and breakage in turbulent Taylor-Couette flow. *J. Colloid Interface Sci.*, 285(1):167–178, 2005.

- [41] S. Whitaker. Flow in porous media I: A theoretical derivation of Darcy's law. *Transport in porous media*, 1(1):3–25, 1986.
- [42] W. Yan, H. Lien, B. E. Koel, and W. Zhang. Iron nanoparticles for environmental clean-up: recent developments and future outlook. *Environmental Science: Processes & Impacts*, 15(1):63–77, 2013.
- [43] L. Zou, L. Jing, and V. Cvetkovic. Modeling of solute transport in a 3D rough-walled fracture–matrix system. *Transport in Porous Media*, 116(3):1005–1029, 2017.